Published in
Applied Physics B: Lasers and Optics 80, issue 7, 841-848, 2005
which should be used for any reference to this work

Light-shift suppression in laser optically pumped vapour-cell atomic frequency standards

C. AFFOLDERBACH[1], C. ANDREEVA[2], S. CARTALEVA[2], T. KARAULANOV[2], G. MILETI[1] ✉, D. SLAVOV[2]

[1]Observatoire Cantonal de Neuchâtel, Rue de l'Observatoire 58, 2000 Neuchâtel, Switzerland
[2]Institute of Electronics, Bulgarian Academy of Sciences, Boul. Tsarigradsko Shosse 72, 1784 Sofia, Bulgaria

ABSTRACT We present a novel scheme for reducing the AC Stark effect in optical-microwave double-resonance spectroscopy and its application for efficient suppression of the light-shift-related instabilities in laser-pumped gas-cell atomic clocks. The method uses a multi-frequency pump light field that can be easily produced by frequency modulation of the single-frequency pump laser. We show theoretically that variations of the light shift with both laser frequency and light intensity can be strongly suppressed with properly chosen pump light spectra. Suitable modulation parameters can be found for both the case of pure frequency modulation as well as for pump light spectra showing amplitude-modulation contributions, as usually found for current modulation of diode lasers. We experimentally demonstrate the method for a Rb atomic clock using a frequency-modulated distributed Bragg-reflector laser diode as pump light source.

1 Introduction

The light shift (LS), also known as the AC Stark effect or optical Stark effect, of an atomic level caused by optical probing is a well-known phenomenon. It arises from the interaction of an induced dipole moment with the oscillating electric field of the light, resulting in a shift of the atomic levels and transition frequencies linear with light intensity in the limit of weak fields [1, 2]. The existence, control, or reduction of the LS plays a crucial role in many fields of fundamental and applied science, for example Sisyphus [3] and Raman sideband cooling [4–6] of atoms in optical lattices [7] or ion-trap quantum information processing [8].

The LS also constitutes one of the main sources of instability in such different types of atomic frequency standards [9] as primary atomic fountain clocks [10, 11], thermal Cs-beam clocks [12], proposed optical frequency standards [13], and vapour-cell atomic clocks based on optical pumping [14, 15] or coherent population trapping (CPT) [16, 17]. A number of different approaches have thus been developed to reduce the AC Stark effect in frequency standards. These rely, for example, on mechanical shutters [10, 18] or rotating 'light traps' [19] to block unwanted laser light in cold-atom clocks, spatial separation of pump and probe regions in Rb masers [20], or the proposed use of optical lattices at 'magic wavelength' that would balance different LS contributions in optical clocks [13].

Here we concentrate on vapour-cell secondary atomic clocks, that offer competitive frequency stabilities both in the short-term (10^{-12} to 10^{-11} at 1 s) and in the long-term scale (10^{-14} to 10^{-11} at one day) within a compact (≤ 0.5 to 2.01), light (≤ 0.5 to 3.5 kg), and low-power (≤ 8 to 35 W) device. These have found a variety of applications in science, telecommunications, industry, and satellite navigation systems (GALILEO, GPS). Schemes developed for the reduction of the LS in such commercial lamp-pumped Rb clocks [9, 14] are mostly based on pulsed optical excitation [21, 22] while, for laboratory prototype clocks based on laser optical pumping [15, 23], the schemes developed rely on spatially separated pump and probe regions [24], pulsed laser pumping [25, 26], or two-frequency laser excitation that balances LS contributions of opposite signs [27]. Schemes developed for CPT-based vapour-cell clocks also balance LS contributions of opposite signs, using laser frequency modulation at 3–5 GHz [16, 28]. Most of these methods, however, either require additional lasers, laser and/or microwave switching, or else compromise the signal contrast, and therefore the clock stability. In fact, limitations due to LS effects and the availability of reliable diode lasers today present the main issues for the development of laser-pumped vapour-cell clocks aiming for stabilities around 10^{-14} on time scales from a few hours up to one day [15, 23].

In this paper we propose and demonstrate a novel method for a practically complete suppression of the LS of the $m_F = 0 \rightarrow 0$ ground-state hyperfine (hf) transition in alkali atoms, discussed here for the case of ^{87}Rb probed in an optically pumped atomic clock. The method utilizes a multi-frequency optical pump light field, obtained in a simple way by frequency modulation of the pump laser. Due to the dependence of the LS on the intensity and frequency of each spectral component, LS contributions stemming from different laser sidebands are

✉ Fax: +41-32-7220420, E-mail: gaetano.mileti@ne.ch

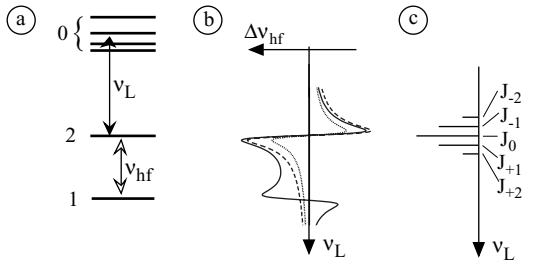

FIGURE 1 **a** Atomic level scheme (the magnetic field dependent $m_F \neq 0$ Zeeman sublevels are not shown). **b** Light shift of the ground-state hf frequency ν_{hf} induced by a single-frequency laser field ν_L scanned around the optical transitions (*solid curve*) and light shift of level 2 only for two different light field powers $P_{L1} > P_{L2}$ (*dashed and dotted lines*, respectively). **c** Spectrum of the frequency-modulated laser for light-shift reduction

of opposite signs and balance each other for suitably chosen modulation parameters. In this respect, the method presented here is similar to LS-reduction strategies studied for the case of CPT-based vapour-cell atomic clocks [16, 28], only it requires much lower modulation frequencies. We present a numerical analysis of the proposed method, as well as the experimental demonstration for an optically pumped Rb gas-cell atomic clock.

2 Description of the method

2.1 *Ground-state light shifts with single-frequency optical pumping*

Figure 1a shows a sketch of the relevant atomic level structure for the case of hf optical pumping frequently performed in alkali atoms. In the case of a ^{87}Rb atomic clock, the frequency difference ν_{hf} between the two ground-state hf 'clock' levels $5\,^2S_{1/2}$, $F_g = 1$, $m_F = 0$ and $5\,^2S_{1/2}$, $F_g = 2$, $m_F = 0$ (labelled 1 and 2, respectively, in Fig. 1a) is probed by a microwave field and subsequently used to stabilize a quartz oscillator that generates the clock signal. Optical pumping on the D_2 line is achieved by a laser field coupling one of the ground-state components to the excited state $5\,^2P_{3/2}$ (labelled 0 in Fig. 1a), whose hyperfine splitting into levels $F_e = 0$, 1, 2, and 3 is not resolved due to strong collisional broadening of the excited states by buffer gases added to the resonance cell for fluorescence quenching, Dicke narrowing [9, 29], and reduction of atom–wall collisions.

Due to the AC Stark shift, the frequency difference ν_{hf} between the two ground-state hf levels 1 and 2 probed in a Rb clock depends on both the power of the pump light field and its frequency (Fig. 1b). The dependence of the LS on laser frequency ν_L exhibits mainly a dispersive shape, where the steep slope at the frequency positions of the levels 1 and 2, quantified by the parameter

$$\beta = \partial\nu_{hf}/\partial\nu_L, \tag{1}$$

characterizes the sensitivity of the hf transition frequency ν_{hf} to laser frequency fluctuations. Similarly, at a fixed light frequency, the dependence of the LS on laser power P_L (dashed and dotted curves in Fig. 1b) is characterized by the coefficient

$$\alpha = \partial\nu_{hf}/\partial P_L. \tag{2}$$

Here we restrict our discussion to the hf LS with dispersive-shape frequency profile and neglect non-dispersive contributions from tensor and Zeeman Stark shifts, which is appropriate for the $m_F = 0 \to 0$ transition in the Rb clock under study and linear pump light polarization [15, 27, 30]. Autler–Townes splittings can be neglected as well, because typical pump light intensities in Rb clocks amount to only a few percent of the saturation intensity of the involved transitions, with even larger margins when collisional broadening and quenching due to a buffer gas are taken into account [9, 31]. (Note that at low light intensities power broadening of the level 2 is also avoided, resulting in typical microwave line widths around 0.3–1 kHz.) For excitation by a single-mode laser field ν_L, the LS profile of one ground-state hf level can be expressed as [27]

$$\Delta_{LS} = \frac{1}{4}\,|\Omega_R|^2\,\frac{\nu_L - \nu_0}{(\nu_L - \nu_0)^2 + \Gamma^2/4}, \tag{3}$$

where Ω_R is the optical Rabi frequency, ν_0 the central frequency, and Γ the width of the optical transition to a single excited-state hf level.

Due to the hyperfine multiplet of the excited state (states 0 in Fig. 1a) the full set of optical transitions starting from the optically pumped ground-state hf level has to be considered [31], as well as the non-resonant transitions starting from the other ground-state levels which give a smaller contribution through the wings of their dispersive LS profiles. Accordingly, for the case of the $F_g = 1$ ground-state level and excitation of the D_2 line of ^{87}Rb, all three transitions starting from the $F_g = 1$ ground-state level, as well as those starting from $F_g = 2$, have to be taken into consideration. The total light shifts $\Delta\nu_1$ and $\Delta\nu_2$ of the $F_g = 1$ and $F_g = 2$ levels, respectively, are

$$\begin{aligned}\Delta\nu_1 &= \frac{1}{4}\sum_{j=0}^{2}|\Omega_{R1j}|^2\,\frac{\nu_L - \nu_{1j}}{(\nu_L - \nu_{1j})^2 + \Gamma^2/4},\\ \Delta\nu_2 &= \frac{1}{4}\sum_{j=1}^{3}|\Omega_{R2j}|^2\,\frac{\nu_L - \nu_{2j}}{(\nu_L - \nu_{2j})^2 + \Gamma^2/4},\end{aligned} \tag{4}$$

where ν_{1j} and ν_{2j} denote the frequency positions of the optical $F_g = 1, 2 \to F_e = j$ transitions. The overall shift $\Delta\nu_{hf}$ of the ground-state hf ('clock') transition is then

$$\Delta\nu_{hf} = \Delta\nu_2 - \Delta\nu_1. \tag{5}$$

In the weak magnetic fields considered here the Zeeman substructure of the hyperfine levels is not resolved for the optical transitions. However, we take into account the Zeeman substructure of the excited-state levels to determine the Rabi frequencies $|\Omega_{R1j}|$ and $|\Omega_{R2j}|$ in Eq. (4) by summing over the appropriate Clebsch–Gordan coefficients for the levels involved with the linear light polarization used here (cf. Sect. 3.1 below).

Figure 2 shows the LS $\Delta\nu_{hf}$ calculated from Eqs. (4) and (5) for excitation by a monochromatic laser field tuned around the $F_g = 2$ transition for different light intensities (frequency splittings are taken from [32, 33]). Due to collisions with the buffer gas in the resonance cell, the excited state is broadened to $\Gamma \approx 1$ GHz and so the excited-state hf structure is not

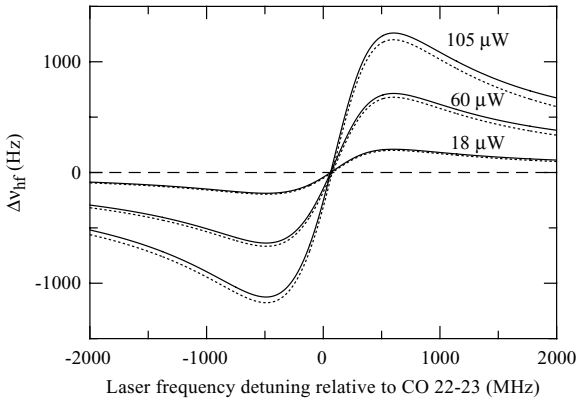

FIGURE 2 Calculated light shift $\Delta\nu_{\rm hf}$ for optical pumping by a single-frequency laser field tuned around the absorption line involving the ^{87}Rb $F_{\rm g} = 2$ level. *Solid and dotted curves* include or neglect the contribution stemming from the non-resonant transition starting from $F_{\rm g} = 1$, respectively. Laser detuning is given relative to the frequency of the cross-over resonance between the transitions $F_{\rm g} = 2 \rightarrow F_{\rm e} = 2$ and $F_{\rm g} = 2 \rightarrow F_{\rm e} = 3$, denoted CO 22-23 in the following (see also Sect. 3.1)

resolved. The total LS profile (solid lines) is slightly asymmetric due to contributions from the off-resonant $F_{\rm g} = 1$ transition (detuned by about 6.7 GHz) which add to the profile from the $F_{\rm g} = 2$ transition alone (dotted lines). For the pump light tuned around the $F_{\rm g} = 1$ transitions, the LS profiles resemble those of Fig. 2, except that the contribution of the off-resonant line is stronger there due to the different transition probabilities, leading to increased asymmetry of the profiles with respect to $\Delta\nu_{\rm hf} = 0$. In both cases, the laser detuning for zero LS $\Delta\nu_{\rm hf} = 0$ is given by the crossing point of the LS profiles for different light intensities. At this laser detuning, the hf transition frequency is insensitive to laser power; thus, $\alpha = 0$. At the same detuning, however, the slope of the LS profiles is steepest (large β-coefficient), so stringent requirements are imposed upon the laser frequency stability if one uses this transition as a precise and stable reference in a Rb clock. The opposite effect occurs for the case when the pump light frequency is tuned to the regions of the extrema of the LS profiles: to first order, the LS frequency dependence vanishes ($\beta \rightarrow 0$), but the laser power dependence is strongest (large α-coefficient).

In state-of-the-art laser-pumped atomic clocks under typical operating conditions, values of the LS coefficients amount to $\alpha \approx 10^{-13}\ \nu_{\rm hf}/\%$ of pump light intensity (with the pump light frequency set within a few megahertz of the zero LS position) and $\beta \approx 5 \times 10^{-11}\ \nu_{\rm hf}$/MHz [15, 23, 30, 34]. In order to reach fractional clock stability goals around 10^{-14} over time scales ranging from a few hours to a day ($\approx 10^4$–10^5 s) required for high-performance applications, such as on-board clocks in satellite navigation systems, it is thus necessary to assure pump light intensity stabilities of $\leq 0.1\%$ and frequency stabilities <1 kHz ($10^{-12}\ \nu_{\rm L}$ in the case of the Rb D_2 line) over the same time period. To guarantee such laser performance in a compact and robust instrument represents a challenging task [35], so strategies to reduce the LS coefficients are of great interest: this would either allow one to improve the stability performance of laser-pumped Rb clocks, or to relax the exacting requirements on the laser intensity and frequency stability mentioned above while maintaining the stability of the clock itself.

The following discussion will address three topics: first, we will demonstrate how to reduce β at the centre of the line profile. In a second step, we show in addition how α can be reduced at the same time, suppressing the sensitivity of the hf microwave transition to variations in both frequency and intensity of the pump light. The last part discusses the influence of residual laser amplitude modulation on the schemes.

2.2 *Light-shift suppression by optical pumping with a multi-frequency light field*

2.2.1 LS β suppression via frequency-modulation sidebands. Consider the excitation of the optical transition from one ground-state hf level by means of a multi-frequency laser field (Fig. 1c) produced by frequency modulation of a single-frequency laser. The total LS of the hf transition is now given by a sum over Eq. (5), taking into account the relative frequencies and optical powers of all sidebands, given by the modulation frequency $\Omega_{\rm M}$ and the modulation index m. Numerical simulation results for a modulation frequency $\Omega_{\rm M} = \Gamma/2 = 500$ MHz are shown in Fig. 3, where the LS curves are presented for different modulation indices. A special case is the LS curve obtained for a modulation index of $m \approx 2.4$, corresponding to zero amplitude of the carrier frequency: here, no LS contribution arises from the depleted carrier, the negative-order sidebands give rise to a negative change of $\nu_{\rm hf}$, and for the positive-order ones the shift is positive. Thus, for a completely symmetric LS profile the sideband contributions cancel out. When the first-order sidebands coincide with the extrema of the light-shift profile, where β is essentially zero, only a small contribution to β stemming from the off-resonant transitions remains. Indeed, the calculations based on Eq. (5) show a strongly reduced β around the line centre (see Fig. 3). Furthermore, if the laser frequency comb drifts by a small amount compared to the optical transition line width, the changes in light-shift contributions from the positive and negative sidebands largely compensate each other in such a way that the overall LS hardly changes at all. This gives rise to an entire frequency interval spanning a few

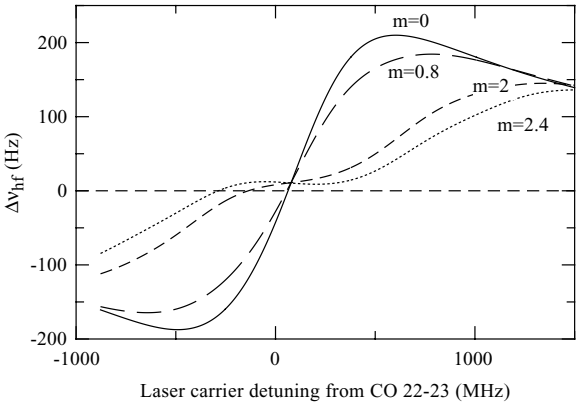

FIGURE 3 Calculated light shift $\Delta\nu_{\rm hf}$ for multi-frequency optical pumping around the $F_{\rm g} = 2$ transitions with different modulation indices. The optical power is $P_{\rm L} = 18\ \mu$W and the modulation frequency is $\Omega_{\rm M} = \Gamma/2 = 500$ MHz

hundred megahertz over which the LS is practically constant with laser frequency, observed as a flat region at the profile centre in Fig. 3. We shall refer to this interval of suppressed LS β as the 'self-correction plateau' in the LS profile.

Note that in the scheme discussed here the modulation frequency is small enough ($\Omega_M \approx 500\,\text{MHz} \ll \nu_{hf} \approx 6.8\,\text{GHz}$) not to introduce ground-state hf coherences via optical transitions starting from the second (non-resonant) hf component, but large enough to avoid the creation of coherences between Zeeman sublevels within a single hf component, which are split by less than 1 MHz by the weak magnetic field applied. Accordingly, in spite of the high degree of coherence between the modulation sidebands (essentially limited by the properties of the modulation source only), no significant coherence effects like CPT are expected here which could compromise the optical pumping efficiency [27, 36]. The use of a frequency-modulated pump light field has also been shown to allow for increased optical pumping efficiency [37]. This impact of the proposed method was, however, not studied there.

It should be noted that in Fig. 3 the crossing point of all curves and the LS in the self-correction plateau with $\beta \approx 0$ are not at zero LS level due to the influence of the hf transitions starting from $F_g = 1$. This offset amounts to about 10 Hz, i.e. $\approx 1.5 \times 10^{-9}$ of the hf transition frequency ν_{hf} here, and also depends on the laser power (non-zero α). It is therefore undesirable in high-stability atomic clocks and it too should be suppressed.

2.2.2 Compensation for LS offset towards $\alpha = 0$. While the LS offset caused by the off-resonant transition is rather small for pumping on the $F_g = 2$ transition, it is much larger when the pump laser is tuned around the $F_g = 1$ transition. However, this offset can be significantly suppressed in a different modulation configuration (see Fig. 4). With the modulation frequency increased to $\Omega_M = 0.7\,\Gamma > \Gamma/2$, the modulation indices $m \approx 2.13$ and $m \approx 2.82$ both result in a small fraction of the overall power contained in the carrier. At a suitable carrier detuning of some 400 MHz from the CO 22-23 resonance, a configuration is found where the contributions of the carrier and one of the first-order sidebands compensate the LS of the other first-order sideband and the contribution stemming from the off-resonant transitions. As a consequence, the LS curve

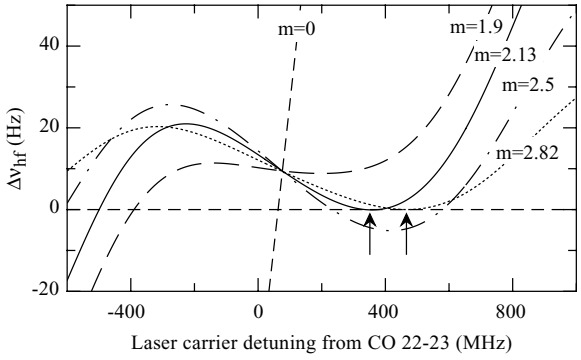

FIGURE 4 Compensation of the self-correction plateau offset on the $F_g = 2$ transition for different modulation indices. The *arrows* indicate regions of low-intensity light shift ($\alpha \approx 0$) for appropriate modulation indices m. The parameters of the model are $\Omega_M = 0.7\,\Gamma = 700\,\text{MHz}$ and $P_L = 18\,\mu\text{W}$

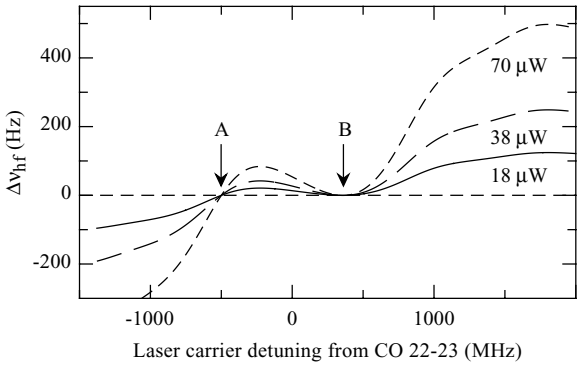

FIGURE 5 Calculated light shift around the $F_g = 2$ transition for different pump light powers. The parameters of the model are $m = 2.13$ and $\Omega_M = 0.7\,\Gamma = 700\,\text{MHz}$. Point A: carrier detuning with $\alpha = 0$, $\beta \neq 0$. Region B: plateau with both $\alpha = 0$ and $\beta = 0$

approaches a zero value not only at a certain point, but over an entire interval, found around a laser detuning of ≈ 400 MHz (arrows in Fig. 4). While this compensation of the LS offset compromises the extension of the flat plateau (compare the plateau in Fig. 3 to the regions indicated by the arrows in Fig. 4), the $\Delta\nu_{hf}$ dependence on laser frequency is only a second-order one and there still exists a frequency interval of more than 200 MHz where the β-coefficient is strongly reduced. In this same frequency interval the LS variation with light intensity—i.e. the α-coefficient—is reduced, too, as is obvious from Fig. 5.

2.2.3 Influence of residual amplitude modulation. Current modulation of diode lasers not only results in frequency modulation of the light field but also causes a certain degree of amplitude modulation, frequently referred to as residual amplitude modulation, which results in a significant difference in the intensities of the positive ($n > 0$)- and negative ($n < 0$)-order sidebands J_n [38]. This asymmetry in the light spectrum depends on the amplitude-modulation depth m_A and the relative phase between frequency and amplitude modulations, and destroys the balancing of light-shift contributions from positive- and negative-order sidebands discussed in Sects. 2.2.1 and 2.2.2. Thus, in the presence of amplitude modulation, an additional LS offset from zero level arises, which increases with increasing amplitude-modulation depth. This is illustrated by the simulations of Fig. 6, which start from the case of a compensated α-coefficient (cf. Fig. 4, $m = 2.13$) but also include different levels of amplitude modulation.

It is possible to compensate for this additional LS offset introduced by amplitude modulation and obtain a zero-LS interval at an appropriate detuning of the laser carrier from the resonance centre in two ways: first, with $\Omega_M > \Gamma/2$ even a large amplitude-modulation depth m_A can be compensated by increasing both the frequency-modulation index m and the frequency Ω_M, similar to the compensation of the offset originating from the off-resonant transition discussed in Sect. 2.2.2. However, we do not consider this approach particularly useful because, at $\Omega_M \gg \Gamma/2$ and large Ω_M, the major part of the laser power will be distributed towards high-order sidebands, which lie far from resonance and contribute only weakly to the optical pumping process, thus compromising the signal-to-noise ratio of the clock signal.

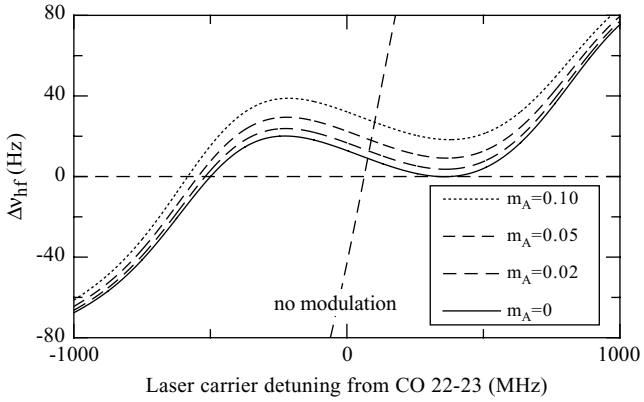

FIGURE 6 Breaking of the zero-LS interval due to different levels of amplitude modulation in the laser light. The parameters of the model are identical to those of Fig. 4

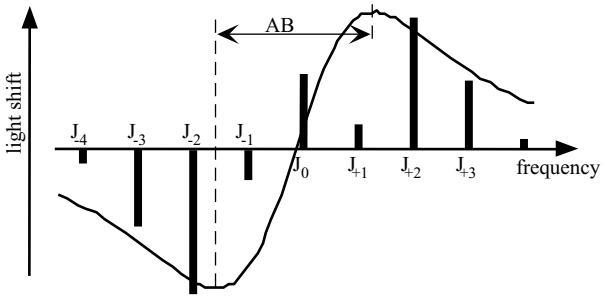

FIGURE 7 Modulation configuration for LS suppression in the presence of residual amplitude modulation. With respect to the centre of the LS profile, the carrier is slightly detuned towards the sidebands with lower intensity (i.e. higher frequency here). The bars indicate the relative sideband intensities

Here, we consider a second possibility with $\Omega_M \lesssim \Gamma/2$ which is more advantageous with respect to optical pumping and whose modulation configuration is sketched in Fig. 7 for the case of a single optical transition. The LS offset due to the asymmetry between equal-order positive and negative sidebands can be compensated when the carrier has non-zero intensity and is detuned towards the lower-intensity sidebands with respect to the centre of the transition. In order to obtain this balance not only at a specific carrier detuning but over a larger frequency interval, the contributions to the β-coefficient from the frequency components lying within the interval of positive LS slope ($\beta > 0$, denoted AB in Fig. 7) should be compensated by those of the components with $\beta < 0$ lying outside this interval. Because of the larger value of $|\beta|$ close to the line centre compared to outside the interval AB, a significant intensity in the sidebands of order $|n| \geq 2$ is required, leading to a value of m around 3.0–3.5. As in practice the LS curve is rather asymmetric due to the hf substructure of the atomic transition investigated, slight variations in sideband configurations will be required to achieve optimum LS compensation for each case.

Figure 8 shows simulation results for a modulation configuration including amplitude modulation as depicted in Fig. 7, taking into account the entire hf structure of the ^{87}Rb D_2 line and laser modulation parameters corresponding to experimental conditions. One can clearly see that the LS is suppressed over an interval of several hundred megahertz with both $\alpha \approx 0$

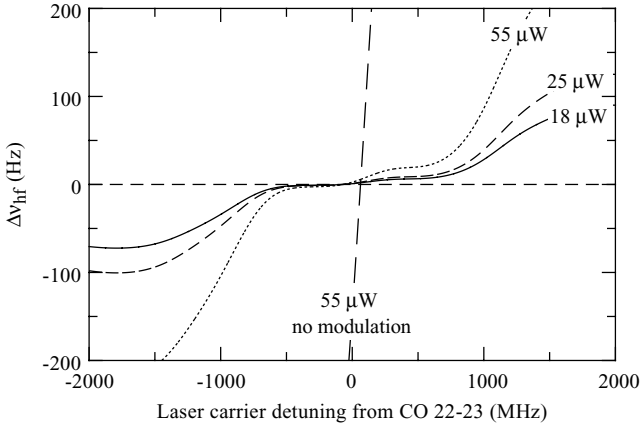

FIGURE 8 Numerical simulation of the light shift around the $F_g = 2$ transitions, including residual amplitude modulation. The parameters of the model are $m = 3.3$, $m_A = 0.035$, and $\Omega_M = 490$ MHz, close to the experimental conditions of Fig. 12. Amplitude and frequency modulations are 180° out of phase, giving maximum sideband asymmetry

and $\beta \approx 0$, even with the residual amplitude modulation taken into account.

3 Experimental verification

3.1 *Experimental set-up*

The experimental set-up used to demonstrate the LS reduction is sketched in Fig. 9 and basically consists of a commercial Rb clock module from which the original discharge lamp producing the pump light was removed. Instead, we use the light emitted from a commercial three-section distributed Bragg-reflector (DBR) laser diode, with a modulation bandwidth large enough to reach the required modulation indices at reasonable radio-frequency (rf) modulation power below 20 dBm. Characterization of the light spectrum was performed via a beat-note measurement against an auxiliary extended-cavity diode laser (not shown in Fig. 9) stabilized to a Rb saturated absorption line. From the measured beat spectra a maximum modulation index of $m \approx 3.5$ was found for modulation of the DBR section at Ω_M around 500 MHz. The main part of the DBR laser beam (linear polarization, cross section 0.35 cm^2) is sent to the clock module, whose resonance cell contains pure ^{87}Rb isotope and a buffer gas. The output frequency of the clock module is compared to an active H-maser reference (Observatoire de Neuchâtel, EFOS) by means of a frequency counter, so we could measure the shift of the

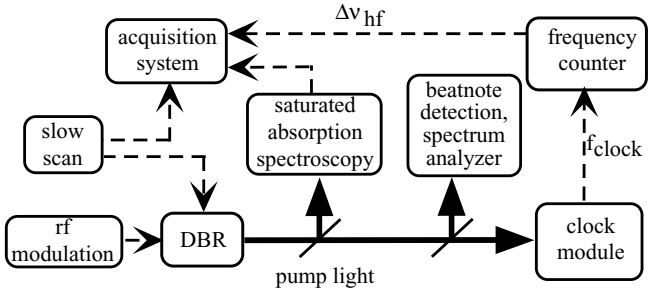

FIGURE 9 Experimental set-up

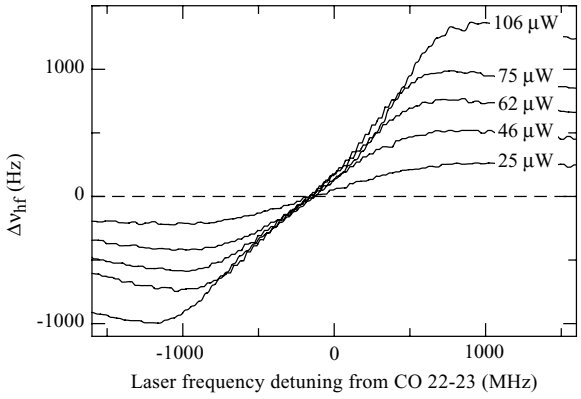

FIGURE 10 Light shift $\Delta\nu_{hf}$ with single-frequency optical pumping on the $F_g = 2$ transition measured for different pump light powers

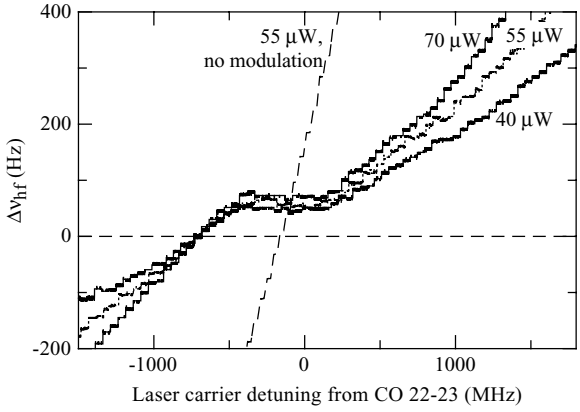

FIGURE 11 Light shift $\Delta\nu_{hf}$ measured with multi-frequency optical pumping on the $F_g = 2$ transition in a ^{87}Rb clock, showing the self-correction plateau of suppressed β ($\Omega_M = 490$ MHz)

atomic microwave transition frequency $\Delta\nu_{hf}$ with a frequency resolution of better than 1 Hz ($\approx 1.5 \times 10^{-10}\Delta\nu_{hf}$). For the LS frequency dependence measurements, the laser frequency was slowly tuned across the atomic resonance and frequency scaling and positioning was achieved by recording simultaneously a reference signal from an auxiliary saturated absorption set-up. The cross-over resonance CO 22-23 between the transitions $F_g = 2 \rightarrow F_e = 2$ and $F_g = 2 \rightarrow F_e = 3$—chosen as the reference for the laser frequency detuning—is easily observed with good contrast in these saturated absorption spectra and also constitutes a suitable reference line for stabilization of the laser frequency in a Rb clock.

3.2 *Experimental results*

3.2.1 Single-frequency optical pumping. Figure 10 shows the measured LS $\Delta\nu_{hf}$ of the hf microwave transition for different laser powers when pumping is performed on the $F_g = 2$ transition with a single-frequency laser field. It can be seen that the zero LS level (defined by the crossing of the curves for different light powers) is not located at the position of symmetry for the LS profiles, indicating the LS contributions from the off-resonant $F_g = 1$ transitions. As in the calculated LS curves, while the shift of the crossing point from the position of symmetry is small here, for pumping on the $F_g = 1$ transition, a larger asymmetry is observed due to the stronger influence of the $F_g = 2$ transitions (not shown). Note that the centre of the LS profiles in the experimental results like Fig. 10 is shifted towards lower frequencies by about 200 MHz due to the buffer gas in the resonance cell (not taken into account in the numerical results of Figs. 2–8).

3.2.2 LS suppression by multi-frequency optical pumping. For experimental verification of the suppression of the β-coefficient, the DBR laser is modulated at $\Omega_M = 490$ MHz $\approx \Gamma/2$, chosen to match the width of the pump transition that is strongly broadened by collisions with the buffer gas. Figure 11 shows the measured LS of the microwave transition for pumping on the $F_g = 2$ transition at different incident pump light powers. At appropriately chosen modulation parameters, we find the self-correction plateau of strongly reduced β-coefficient, showing a width of several hundred megahertz. Note that the plateau is not at zero light-shift level and its offset depends on the laser power, manifesting the still large α-coefficient.

In order to bring the observed plateau offset (about 10% of the maximum light-shift amplitude) to zero LS, i.e. to reduce the α-coefficient also, it was found that a slightly lower modulation frequency of $\Omega_M = 480$ MHz was optimal, as expected from the model simulations. The resulting LS curves depicted in Fig. 12 show a strong suppression of the light shift over a broad frequency interval (about 400 MHz wide). Around zero laser detuning, the LS curves run essentially horizontally and no offset changing with light power is observed there: thus, both the α- and β-coefficients are significantly reduced. Note also that, compared to the case of single-frequency pumping, the LS with multi-frequency pumping is lower in the entire frequency interval recorded (compare Figs. 11 and 12 with Fig. 10).

The experimental results of Fig. 12 are in good agreement with the model predictions of Fig. 8, given for parameters corresponding to the experimental conditions of Fig. 12. Remaining discrepancies concerning, for example, the

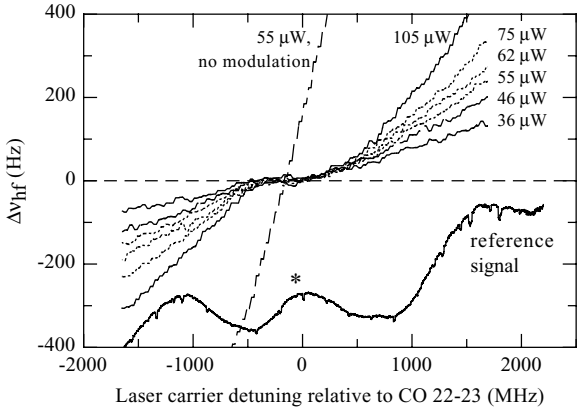

FIGURE 12 *Upper traces*: measured light shift $\Delta\nu_{hf}$ with multi-frequency optical pumping on the $F_g = 2$ transition in a ^{87}Rb clock, demonstrating simultaneous suppression of α- and β-coefficients ($\Omega_M = 480$ MHz). *Lower trace*: corresponding saturated absorption spectrum obtained from the reference cell. The *asterisk* marks a suitable resonance line for laser stabilization within the LS plateau

modulation frequency Ω_M, can be attributed to uncertainties in the experimental values for the modulation parameters m and m_A and the width Γ of the optical transitions. Furthermore, the simulations neglect light absorption in a first part of the vapour cell which does not contribute to the clock signal, but can affect the intensity of the laser sidebands. The experiments confirm that the identified modulation configuration with $m \approx 3.5$ used in the experiment provides a convenient way to overcome limitations imposed by the inevitable amplitude modulation always present in diode lasers, and to finally achieve the zero offset of the self-correction plateau shown in Fig. 12.

Another advantage of this modulation configuration is that at $m \approx 3.5$ the carrier amplitude is large enough for the creation of strong saturated absorption resonances in the reference cell. The bottom trace of Fig. 12 presents such an absorption signal, where the cross-over resonance CO 22-23 induced by the carrier is marked by an asterisk. This resonance is situated within the zero-LS plateau interval and can be used for stabilization of the pump light carrier frequency in a Rb clock.

3.2.3 Quantitative evaluation of the LS reduction. For a quantitative evaluation of the LS reduction, Fig. 13 shows the β-coefficients deduced from the slopes of the LS curves for the case of single-frequency pumping (Fig. 10, around the crossing point) and frequency-modulated pump light (Fig. 12, on the plateau) as a function of pump light power. The strong reduction of the β-coefficient for modulated pump light can be seen in the $\Delta\beta/\Delta P_L$ rate significantly reduced by a factor of 45.

The α-coefficient was determined by stabilizing the laser to appropriate cross-over resonances in the reference cell and measuring $\Delta\nu_{hf}$ at different laser powers. The linear slopes $\Delta\nu_{hf}/\Delta P_L$ obtained are given in Fig. 14, yielding $\alpha_{sf} = 0.81\,\mathrm{Hz}/\mu\mathrm{W}$ for single-frequency pumping at the CO 22-23 resonance. For pumping with modulated light at the same laser carrier frequency, the slope $\Delta\nu_{hf}/\Delta P_L$ lies within the scatter of our measurements (inset in Fig. 14). For a conservative estimate of α, we thus take the standard deviation of this scatter for the slope, which gives $\alpha_{mod} = 1 \times 10^{-2}\,\mathrm{Hz}/\mu\mathrm{W}$. Hence, α is suppressed by a factor of more than 80 when locked to the CO 22-23 resonance.

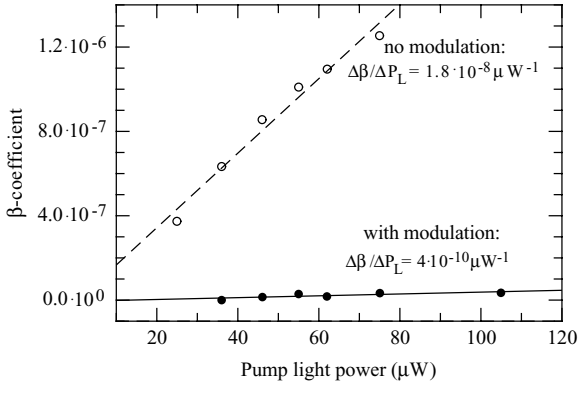

FIGURE 13 Reduction of the β-coefficient for different pump light powers P_L and optical pumping on the $F_g = 2$ transition

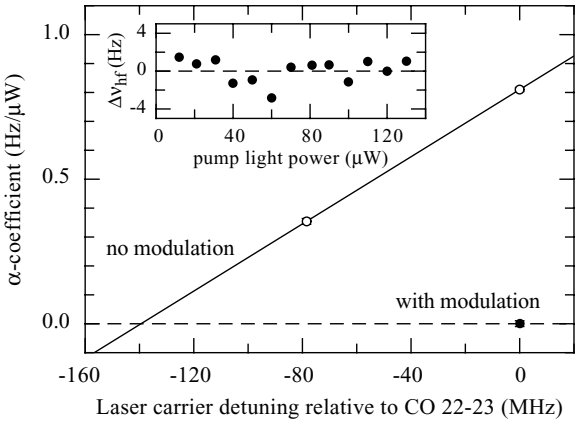

FIGURE 14 Reduction of the α-coefficient for different laser carrier detuning and optical pumping on the $F_g = 2$ transition. The *inset* shows the light-shift dependence on the pump light power measured for the modulated laser stabilized to the CO 22-23 resonance

For the suppression of the LS presented here, the required precision for setting the modulation index m was not found to be very critical. A precision of a few tenths of dBm in the applied radio-frequency modulation power was found to be sufficient, and no significant changes in modulation efficiency of the laser diode used were observed over a period of several months. The precision needed for the modulation frequency Ω_M can easily be guaranteed, too, even with the rather strong dependence of the LS α suppression on Ω_M reported in Sect. 3.2.2. Thus, the required stabilities of the rf modulation parameters over the time scales of interest for a Rb clock are expected to be easily met, also when implementing the method in a Rb clock. However, the amount of residual amplitude modulation can vary between different types of laser diodes and slight variations might even occur between different units of the same type of diode, as is also the case for the diodes' overall modulation efficiency due to, for example, varying coupling efficiencies of the rf power to the diode chip. Some optimization of the modulation parameters for each individual diode implemented will thus be necessary.

We note finally that no significant reduction of the double-resonance signal was observed for the multi-frequency optical pumping compared to the single-frequency case, in spite of the presence of non-resonant spectral components. Thus, our method does not compromise the clock signal and short-term frequency stability.

4 Conclusion

We have demonstrated a novel method for the suppression of the light shift of the ground-state microwave transition in laser-pumped vapour-cell atomic clocks. Significant LS suppression is achieved by pumping with a multi-frequency light field, generated by frequency modulation of the laser source. Such light fields can be conveniently created by current modulation of diode lasers, which overcomes the need for additional, far-detuned lasers involved in other approaches [27].

Our numerical studies show a clear reduction of the LS with respect to changes of both the frequency (β) and intensity (α) of the pump light when suitable frequency modulation

is applied. For depleted carrier intensity and $\Omega_M = \Gamma/2$, the β-coefficient is suppressed and one obtains a self-correction plateau several hundred megahertz wide, where the LS is largely insensitive to laser frequency fluctuations. The offset of the self-correction plateau from zero LS level can be compensated by adapting the modulation parameters. Our experimental results demonstrate this simultaneous suppression of the α- and β-coefficients by factors of 80 and 45, respectively, over a large frequency interval of about 400 MHz. By choosing a high modulation index $m \approx 3.5$, the method also allows us to compensate for residual amplitude modulation that would otherwise compromise the results. In this latter case, the carrier amplitude is strong, thus allowing easy stabilization of the laser frequency within the self-correction plateau, which is relevant for applications in compact Rb atomic clocks or other devices.

While the light-shift reduction was experimentally demonstrated for the case of a Rb atomic clock, the method should be valid in general for all alkali atoms and other systems showing a similar level scheme, including in particular Cs vapour-cell clocks [23]. It has potential application for optically pumped magnetometers using atomic vapour cells [39–41], and possibly even for light-shift control in a wider range of experiments including cold atoms or ions [8] if the modulation frequency were suitably chosen. In particular, by adding modulation sidebands to the preparation and/or detection laser in frequency standards based on cold atoms, LS effects due to the corresponding stray laser light could be suppressed, though not those originating from the atomic fluorescence [19]. In these cases, however, the light-shift contributions neglected in our presented studies will need to be considered in more detail.

ACKNOWLEDGEMENTS This work was supported financially by the Swiss National Science Foundation under Project Nos. 2100-066821.01, R'Equip 2160-067498, and SCOPES 7 BUPJ062412, and by the European Space Agency (ESA) Contract No. 15280/01/NL/US. We thank Temex Neuchâtel Time for providing the clock unit and M.D. Plimmer for careful reading of the manuscript. SC, CA, TK, and DS also thank the Bulgarian National Council for Scientific Research (Grant No. F-1005/00).

REFERENCES

1 J. Barrat, C. Cohen-Tannoudji, J. Phys. Radium **22**, 329 (1961)
2 C. Cohen-Tannoudji, J. Dupont-Roc, G. Grynberg, *Atom–Photon Interactions: Basic Processes and Applications* (Wiley, New York, 1992). Translated from *Processus d'Interaction Entre Photons et Atomes* (InterEditions, Paris, 1988)
3 J. Dalibard, C. Cohen-Tannoudji, J. Opt. Soc. Am. B **6**, 2023 (1989)
4 A.J. Kerman, V. Vuletic, C. Chin, S. Chu, Phys. Rev. Lett. **84**, 439 (2000)
5 A.V. Taichenachev, A.M. Tumaikin, V.I. Yudin, L. Hollberg, Phys. Rev. A **63**, 033402 (2001)
6 G. Di Domenico, N. Castagna, G. Mileti, P. Thomann, A.V. Taichenachev, V.I. Yudin, Phys. Rev. A **69**, 063403 (2004)
7 P. Jessen, I. Deutsch, Adv. At. Mol. Opt. Phys. **37**, 95 (1996)
8 H. Häffner, S. Gulde, M. Riebe, G. Lancaster, C. Becher, J. Eschner, F. Schmidt-Kaler, R. Blatt, Phys. Rev. Lett. **90**, 143 602 (2003)
9 J. Vanier, C. Audoin, in *The Quantum Physics of Atomic Frequency Standards* (Adam Hilger, Bristol, 1989)
10 S.R. Jefferts, J. Shirley, T.E. Parker, T.P. Heavner, D.M. Meekhof, C. Nelson, F. Levi, G. Costanzo, A. De Marchi, R. Drullinger, L. Hollberg, W.D. Lee, F.L. Walls, Metrologia **39**, 321 (2002)
11 A. Joyet, G. Mileti, P. Thomann, G. Dudle, in *Proceedings of the 6th Symposium on Frequency Standards and Metrology*, ed. by P. Gill (World Scientific, Singapore, 2001), p. 273
12 A. Makdissi, J.-P. Berthet, E. de Clercq, IEEE Trans. Ultrason. Ferroelectr. Freq. Control **47**, 461 (2000)
13 H. Katori, M. Takamoto, V.G. Pal'chikov, V.D. Ovsiannikov, Phys. Rev. Lett. **91**, 173 005 (2003)
14 J.C. Camparo, R.P. Frueholz, C.H. Volk, Phys. Rev. A **27**, 1914 (1983)
15 G. Mileti, J. Deng, F.L. Walls, D.A. Jennings, R.E. Drullinger, IEEE J. Quantum Electron. **34**, 233 (1998)
16 F. Levi, A. Godone, J. Vanier, IEEE Trans. Ultrason. Ferroelectr. Freq. Control **47**, 466 (2000)
17 S. Knappe, R. Wynands, J. Kitching, H.G. Robinson, L. Hollberg, J. Opt. Soc. Am. B **18**, 1545 (2001)
18 C. Fertig, K. Gibble, B. Klipstein, L. Maleki, D. Seidel, R. Thompson, in *Proceedings of the 2000 IEEE Frequency Control Symposium*, ed. by J. Vig (Institute of Electrical and Electronics Engineers, Piscataway, 2000), p. 676
19 A. Joyet, N. Castagna, P. Thomann, G. Dudle, C. Mandache, T. Ascente, in *Proceedings of the 2003 IEEE Frequency Control Symposium jointly with the 17th European Frequency and Time Forum*, ed. by J.R. Vig (Institute of Electrical and Electronics Engineers, Piscataway, 2003), p. 115
20 W.M. Golding, A. Frank, R. Beard, J. White, F. Danzy, E. Powers, in *Proceedings of the 48th IEEE Frequency Control Symposium*, ed. by J.R. Vig (Institute of Electrical and Electronics Engineers, Piscataway, 1994), p. 724
21 C.O. Alley, in *Quantum Electronics*, ed. by C.H. Townes (Columbia University Press, New York, 1960), p. 146
22 T.C. English, E. Jechart, T.M. Kwon, in *Proceedings of the 10th Precise Time and Time Interval Systems and Applications Meeting*, ed. by L.J. Rueger (Goddard Space Flight Center, Greenbelt, 1978), p. 147
23 Y. Ohuchi, H. Suga, M. Fujita, T. Suzuki, M. Uchino, K. Takahei, M. Tsuda, Y. Saburi, in *Proceedings of the 2000 IEEE Frequency Control Symposium*, ed. by J. Vig (Institute of Electrical and Electronics Engineers, Piscataway, 2000), p. 651
24 M. Feldman, J.C. Bergquist, L.L. Lewis, F.L. Walls, in *Proceedings of the 35th IEEE International Frequency Control Symposium*, ed. by E. Hafner (Electronic Industries Association, Washington, DC, 1981), p. 625
25 N.D. Bhaskar, IEEE Trans. Ultrason. Ferroelectr. Freq. Control **42**, 15 (1995)
26 A. Godone, S. Micalizio, F. Levi, Phys. Rev. A **70**, 023409 (2004)
27 J. Deng, IEEE Trans. Ultrason. Ferroelectr. Freq. Control **48**, 1657 (2001)
28 M. Zhu, L.S. Cutler, in *Proceedings of the 32nd Precise Time and Time Interval Systems and Applications Meeting*, ed. by L.A. Breakiron (US Naval Observatory, Washington, DC, 2000), p. 311
29 R.H. Dicke, Phys. Rev. **89**, 472 (1953)
30 B. Mathur, H. Tang, W. Happer, Phys. Rev. **171**, 11 (1968)
31 M. Arditi, J.-L. Piqué, J. Phys. B: At. Mol. Phys. **8**, L331 (1975)
32 J. Ye, S. Swartz, P. Jungner, J.L. Hall, Opt. Lett. **21**, 1280 (1996)
33 S. Bize, Y. Sortais, M.S. Santos, C. Mandache, A. Clairon, C. Salomon, Europhys. Lett. **45**, 558 (1999)
34 G. Mileti, J.Q. Deng, F.L. Walls, J.P. Lowe, R.E. Drullinger, in *Proceedings of the 1996 IEEE International Frequency Control Symposium*, ed. by K. Yamanouchi, J. Vig (Institute of Electrical and Electronics Engineers, Piscataway, 1996), p. 1066
35 C. Affolderbach, G. Mileti, D. Slavov, C. Andreeva, S. Cartaleva, in *Proceedings of the 18th European Frequency and Time Forum* (The Institution of Electrical Engineers, Stevenage, 2004), p. 84
36 E. Arimondo, Prog. Opt. **35**, 257 (1996)
37 P. Tremblay, J. Beaubien, A. Michaud, E. Cauchon, J. Opt. Soc. Am. B **9**, 1537 (1992)
38 S. Kobayashi, Y. Yamamoto, M. Ito, T. Kimura, IEEE J. Quantum Electron. **18**, 582 (1982)
39 E.B. Aleksandrov, V.A. Bonch-Bruevich, N.N. Yakobson, Sov. J. Opt. Technol. **60**, 754 (1993)
40 G. Bison, R. Wynands, A. Weis, Appl. Phys. B **76**, 325 (2003)
41 Yu.P. Malakyan, S.M. Rochester, D. Budker, D.F. Kimball, V.V. Yashchuk, Phys. Rev. A **69**, 013817 (2004)